Article

Bimetallic [Co/K] hydrogen evolution catalyst for electrochemical terminal C-H functionalization

Sheng Zhang [1]✉, Lei Hong [1], Jiayi Feng [1], Mohan Wang [1], Junyuan Hu [2], Ying Zhang [1] & Man-Bo Li [1]✉

Discovering novel catalysts for hydrogen evolution reaction (HER) holds the potential to revolutionize the energy chemistry and unlock new tool for synthetic processes. Inspired by hydrogenases, we pair alkali metals with cobalt-Salen catalysts which allow the integration of naked base site into bimetallic HER catalysts. The incorporation of alkali metals (Na, K, Rb, Cs) significantly enhances HER activity. Among these, the [Co/K] system exhibits the highest HER catalytic efficiency (k_{obs} ~ 31.4 s^{-1}), which is 9 times higher than the mononuclear analogue. Remarkably, this HER catalyst is repurposed for the terminal C(sp^3)-H functionalization of N-allylimines with imine/aldehyde, a previously inaccessible transformation. Mechanistic studies reveal that the naked base site enables selective C-H activation via proton relay, overriding the inherent preference for Pinacol coupling. The electrochemical protocol features good functional group tolerance, and opens up a streamlined avenue for chiral pyrrolines, key precursors of the anti-cancer medicine Larotrectinib. More importantly, the alkali metal effect is rationalized through structural analysis, density functional theory (DFT) calculations, and control experiments.

Developing highly efficient catalysts for the hydrogen evolution reaction (HER)[1–4] is one of the central topics in energy chemistry, since hydrogen can be considered an ideal surrogate for fossil fuels. Natural [NiFe]- and [FeFe]-hydrogenases[5,6] achieve high HER activity through synergistic bimetallic centers and proton-relaying base sites (Fig. 1a). These two factors have been individually leveraged to facilitate the HER catalyst discoveries. The bimetallic[7–10] strategy has been widely explored and well-documented in the hetero-[11,12] and homogeneous[13–15] HER catalyst discovery (Fig. 1b). Meanwhile, the proton relay strategy[16,17] has proven highly effective in molecular HER catalysts, as demonstrated in the compelling reports[18–21] (Fig. 1b). Nevertheless, integrating proton relay sites into bimetallic HER catalysts has received far less attention[22]. With our long-term research interest[23–26] in cobalt-Salen[27–31] HER catalysis, we envisaged that its modular structure could

serve as an ideal platform for developing such bimetallic HER catalysts (Fig. 1c). The less explored alkali metals (AM)[32,33] were selected to combine with cobalt-Salen systems, given their low toxicity and strong hydride affinity, which would lead to more reactive metal hydride for HER catalysis. Moreover, the interaction between alkali metals and oxygen sites can release a naked base site, enabling rapid proton transfer during HER. Guided by this concept, we devised a series of cobalt/alkali-Salen catalysts bearing naked base sites, and potassium ion demonstrated an unmatched enhancement in HER efficiency.

The robust bimetallic HER catalyst offers an unconventional tool[34–40] for electrochemical C−H functionalization[23–26,41–47], as it can break sp^3 C−H bonds into the relative carbanion species while simultaneously releasing H$_2$. The functionalization of N-allylimine[48–52] with imines provides direct access to various bioactive amines, including

[1]Institutes of Physical Science and Information Technology, Key Laboratory of Structure and Functional Regulation of Hybrid Materials of Ministry of Education, Anhui University, Hefei, Anhui, China. [2]School of Chemistry and Chemical Engineering, Shandong University, Jinan, China. ✉e-mail: shengzhang@ahu.edu.cn; mbli@ahu.edu.cn
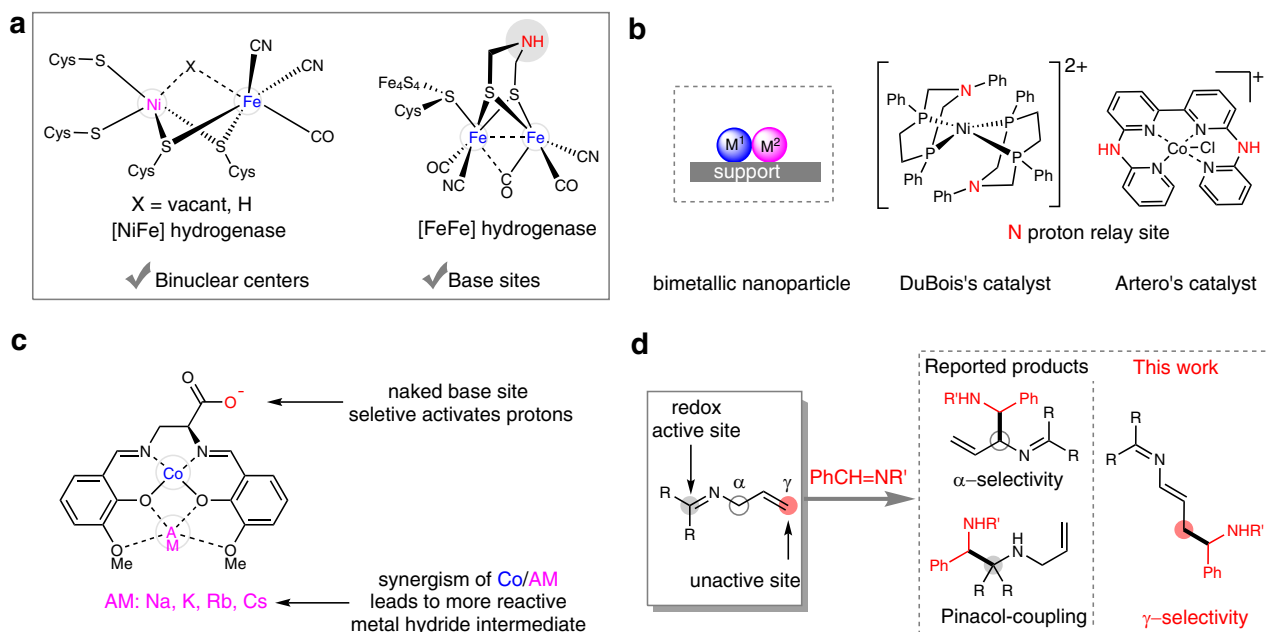
Fig. 1 | Strategies for HER catalyst finding and the C−H functionalization of *N*-allylimine. a The structure of [NiFe] and [FeFe] hydrogenases. **b** Reported strategies for HER catalysts. **c** The structure of cobalt/alkali-Salen HER catalyst. **d** The C−H functionalization of *N*-allylimine. AM alkali metal.

both α- and γ-selective products (Fig. 1d). Conventional protocol[52] involving excessively strong base *ⁿ*BuLi and the activator *N,N,N′,N′*-tetramethylethylenediamine (TMEDA) predominantly yields α-selective products. Selectively accessing terminal C−H (γ-C−H) functionalized products remains a formidable challenge, although this unconventional product allows a straightforward pathway to diverse chiral pyrrolines, which are widespread in 40 U.S. FDA-approved drugs[53] and amino organocatalysts[54]. In this context, we envisaged that the developed bimetallic HER catalysts might address the challenge of terminal C−H selectivity in this reaction. However, the electrochemical C−H functionalization of *N*-allylimine faces inherent challenges. That is, the *N*-allylimine substrate preferentially couples with imines or aldehydes to give Pinacol coupling[55−57] products under electroreduction, owing to its redox-active imine moiety (Fig. 1d). In contrast, C−H bonds of *N*-allylimine are poor acidic (pKa > 30) and typically considered redox-unactive. This contradiction poses a great obstacle for electrochemical C−H functionalization of *N*-allylimine.

In this work, we unveil that the bimetallic [Co/K] catalyst[58] overcomes this inherent limitation by selectively activating C−H bonds with a naked base site and efficiently breaking C−H bonds with in situ formed Co/K hydrides. This electrocatalytic protocol exhibits several impressive advantages, including good functional group tolerance, high stereoselectivity, mild reaction conditions, and good scalability. The versatility of the [Co/K] catalyst is further extended to the terminal C−H functionalization of *N*-allylimine with aldehydes.

Results

The catalysts synthesis and catalytic activity evaluation

We set out to synthesize the bimetallic cobalt/alkali-Salen catalyst via a one-pot procedure (Fig. 2a). The Salen ligand was prepared through the direct condensation between (*L*)−3-aminoalanine hydrochloride and two equivalents of o-vanillin using various alkali metal hydroxides as base at 50 °C. Further treatment with cobalt acetate and an additional two equivalents of base gave the desired bimetallic complexes as a colored precipitate, which can be directly used for catalysis after a hot filtration. To our delight, this approach is amenable to give a series of alkali metals (Na, K, Rb, Cs) bimetallic catalysts on a gram scale. Nevertheless, lithium hydroxide failed to give the desired complex,

presumably due to its mismatched ionic radius. These bimetallic catalysts were unambiguously characterized by nuclear magnetic resonance (NMR) (Figs. S2–S9) and high-resolution mass spectrometry (HRMS). It reveals that the methoxy anion coordinates with the cobalt center as an extra ligand. This structure assignment was also verified by the single-crystal diffraction analysis of **cat 2** (Deposition number 2422475 (for **cat 2**) contains the supplementary crystallographic data for this paper. These data are provided free of charge by Cambridge Crystallographic Data Centre). As depicted in Fig. 2b, the potassium ion is firmly chelated by four oxygen atoms to release a free carboxylate anion. The resulting structure resembles a scorpion, with a potassium 'head' and a carboxylate 'tail'. In the solid state, the bimetallic complexes dimerize readily via a head-to-tail connection.

With the structurally well-defined bimetallic catalysts, we next probed the influence of alkali metals on the cobalt center by conducting a comparative analysis of the chemical shift of surrounding proton H^a and H^b (Fig. 2c). A consistent trend in the variation of chemical shifts was observed for both protons. The stronger the metallic character of the alkali metal (Cs > Rb > K > Na), the more electron-rich the cobalt center became. This increase in electron density is expected to generate more alkaline metal hydride species, thereby enhancing the efficiency of the hydrogen evolution reaction. Subsequently, we evaluated the electrochemical properties of the catalysts using a relevant cobalt-Salen (**cat 5**) as a reference. The redox potentials corresponding to $Co^{III/II}$ and $Co^{II/I}$ processes were identified (Figs. S11–S15) and summarized in Fig. 2d. It clearly shows that alkali metals significantly change the electrochemical behaviors of Salen catalysts (**cat 1**–**cat 4**) compared to **cat 5**. The redox couples of $Co^{III/II}$ uniformly shifted to more negative potentials, which might be ascribed to the steric hindrance and electronic effect of the carboxylate anion. On the other hand, the potential of $Co^{II/I}$ decreased with the increasing metallicity of the alkali metals; potassium, rubidium, and cesium resulted in more negative peaks than that of **cat 5**. Subsequently, we investigated the effect of alkali metals on the HER catalytic performance using a glassy carbon (GC) electrode in DMF solution with acetic acid as a proton source (Fig. 2e). Upon treating with the acid, the reduction waves associated with $Co^{II/I}$ were enhanced dramatically. We quantified the current increment with the ratio (i_c/i_p) of the catalytic
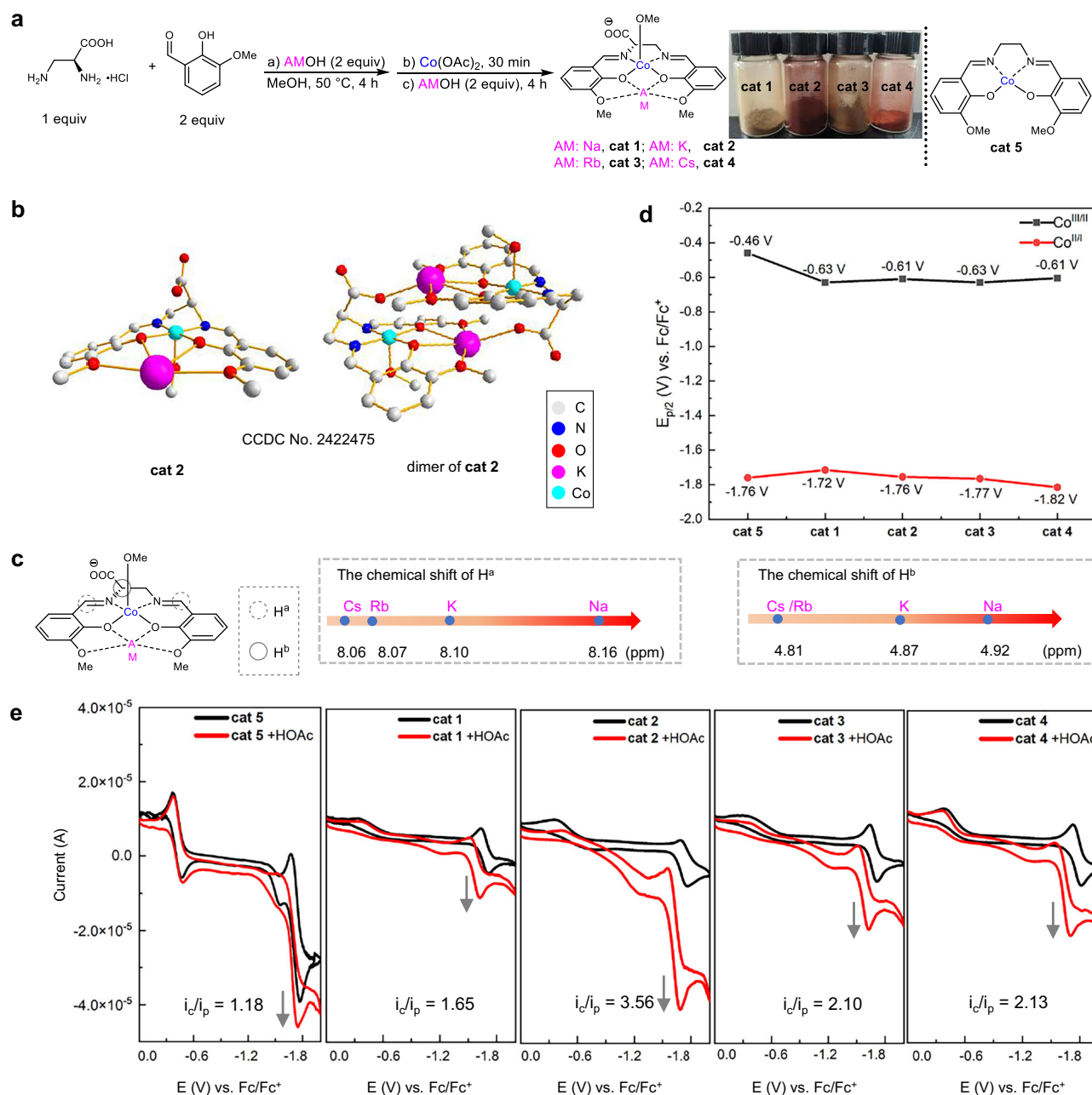
Fig. 2 | Synthesis and HER activity of cobalt/alkali-Salen catalysts. a Synthetic route of cobalt/alkali-Salen catalysts. **b** Single-crystal structure of **cat 2**. **c** The chemical shifts of the protons in the HER catalys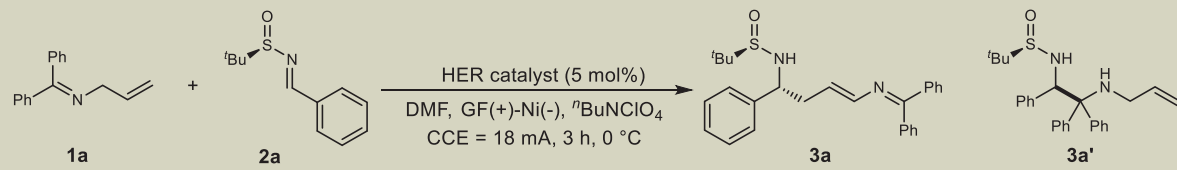ts. **d** Redox potentials of catalysts. **e** Cyclic voltammograms of HER catalyst (0.01 mmol) and acetic acid (0.175 mmol) in DMF (3.0 mL) solution with $^nBuNClO_4$ as electrolyte. DMF *N,N*-dimethylforma-mide, Fc ferrocene.

current and peak current. The result indicates that bimetallic HER catalysts (**cat 1**–**cat 4**) exhibited higher efficiency than the reference catalyst, **cat 5**. Notably, the [Co/K] catalyst (**cat 1**) was recognized as the most efficient one, displaying the highest i_c/i_p value (3.56) and a 9-fold higher rate constant ($k_{obs} = 31.4\,s^{-1}$) compared to **cat 5** ($k_{obs} = 3.5\,s^{-1}$). This result underscores the critical role of the appropriate metallicity and ionic radius of alkali metals in contributing to both the structural stability of the metal framework and the reactivity required for H_2 production. Additionally, the gas chromatography (GC) experiment further verified the hydrogen product during the electrolysis (Fig. S32).

Reaction optimization and substrate scope examination

Encouraged by the promising HER catalytic performance, we sought to access unconventional terminal C−H selectivity in the reaction between *N*-allylimine (**1a**) and Ellman imine[59] (**2a**). Initially, we conducted the reaction in the absence of any catalysts using graphite felt anode and nickel cathode with DMF as solvent (Entry 1, Table 1). As expected, the corresponding cross-Pinacol coupling product **3a'** was delivered in 21% yield along with some homo-coupling byproduct. Variations on other electrolysis parameters, such as electrolyte and solvent, failed to afford the desired C−H functionalization product (for details, see Table S2). Gratifyingly, introducing HER catalysts substantially changed the reaction selectivity (Entry 2–6). The desired terminal C−H selective product **3a** was exclusively accessed by using **cat 5**, albeit with only 30% yield (Entry 2). Further modifications on the structure of mononuclear Salen catalyst have a negligible impact on the reaction efficiency (Table S2). In contrast, bimetallic cobalt/alkali-Salen catalysts showed great enhancement in the reaction yield, which is in good consistency with the HER activity evaluation. The highest

Table 1 | Optimization of reaction conditions[a]

Entry	Variations of reaction conditions	Product	Yield (%)[b]
1	No HER catalyst	**3a'**	21
2	**cat 5** as HER catalyst	**3a**	30
3	**cat 1** as HER catalyst	**3a**	50
4	**cat 2** as HER catalyst	**3a**	81
5	**cat 3** as HER catalyst	**3a**	68
6	**cat 4** as HER catalyst	**3a**	71
7	No electricity[c]	-	-
8	**cat 2** as HER catalyst, zinc plate as anode	**3a**	52

GF graphite felt, *CCE* constant current electrolysis, *DMF* N,N-dimethylformamide.
[a]Reaction conditions: **1a** (1.5 mmol), **2a** (0.5 mmol), HER catalysts (5 mol%), ^{n}Bu$_4$NClO$_4$ (1.0 mmol), DMF (10 mL), graphite felt anode, nickel plate cathode, undivided cell, CCE = 18 mA, 3 h (4.03 F/mol), 0 °C.
[b]Isolated yield, reaction diastereoselectivity (*dr*) >15/1, *E/Z* > 20/1;
[c]48 h.

activity was observed for the [Co/K] complex (**cat 2**), and the desired product **3a** was afforded in 81% yield (Entry 4). The reaction monitoring experiment (Table S3) further demonstrates that the HER catalyst (**cat 2**) exhibits high initial catalytic efficiency and maintains good durability under progressively basic reaction conditions. The control experiment (Entry 7), removing electricity directly shut down the reaction even with prolonged reaction time (48 h), implying the necessity of electricity. Replacing the graphite felt anode with a sacrificial zinc anode largely maintained the reaction yield (52%). This suggests that the terminal C–H selective product **3a** should be generated via cathodic electrolysis (Entry 8).
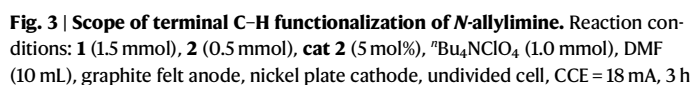
Following systematic optimization, we next examined the protocol generality with variations on both substrates. A broad range of the Ellman imines was first subjected to the optimal conditions (Fig. 3). The electronic effect investigation revealed that electron-deficient substrates (**3h-3m**) gave the desired product with slightly higher yields compared to the electron-rich ones (**3b-3g**). Some useful but conventionally challenging substituents (e.g., thioether, amine, vinyl, iodine, ester) were amenable to give the terminal C–H functionalization product in moderate to good yields (**3n-3r**). Notably, this method showed excellent tolerance for other fused rings (**3s-3u**) and medicinally relevant heterocycles, including quinoline (**3v**), pyridine (**3w**), thiophene (**3x-3y**), and imidazole (**3z**). Moreover, ferrocene (**3aa**), as a key moiety of functional materials, proved to be suitable in the transformation. The protocol compatibility for substituent patterns (**3ab-3am**) was also tested, and the reaction efficiency was largely maintained. Specifically, substrates bearing bulky groups, such as 2-diphenylphosphino (**3ah**), 2-allyloxy (**3ai**), 2,6-methyl (**3aj**), and chlorine (**3ak**) still reacted smoothly, although they resulted in lower diastereoselectivity. Bioactive fluorinated imines furnish the desired products (**3al-3am**) in 79% and 62% yields, respectively. Aliphatic imine (**3an**) and diaryl ketimine (**3ao**) resulted in deteriorated reaction performance, whereas it should be noted that the radical-sensitive cyclopropyl ring was intact after electrolysis, supporting an ionic reaction pathway. Furthermore, the mildness of the method allows a facile platform for the late-stage functionalization of pharmaceutical (Adapalene **3ar**) and natural products (Diacetonefructose **3ap**, Vitamin E **3aq**, Cholesterol **3as**) that bear multiple functional groups.

Nevertheless, Ellman imines (**2at-2au**) with acidic α-C–H were found to be unsuccessful in the reaction since it would interfere with the HER of *N*-allylimine C–H. The scope of *N*-allylimines was also tested by varying β-substituents. Alkyl groups afforded the corresponding products (**3at-3au**) in good stereocontrol, while aryl groups (**3av-3bc**) led to lower *E/Z* selectivity owing to its similar steric hindrance compared with the sulfinamide moiety in the product. *N*-homoallylimine **1bd** with a poor acidic C–H bond was found to be incompatible in the transformation.

To further demonstrate the robustness of the [Co/K] catalyst, we extended its application to the terminal C–H functionalization of *N*-allylimines with aldehydes. As shown in Fig. 4a, high reaction efficiency and excellent functional group tolerance (**4a-4t**) were readily achieved merely with 2 mol% catalyst loading. Intriguingly, *N*-allylimine containing diene moiety was competent, and the terminal C–H was selectively functionalized with benzaldehyde to give a new product **4t**. We next investigated the scalability of the electrocatalytic approach (Fig. 4b). Under simply modified reaction conditions, 5 mmol scale reactions of both benzaldehyde and Ellman imine (**2a**) proceed smoothly to couple with **1a**, affording respective products **4a** and **3a** in acceptable yields. Finally, the derivatization of products to chiral pyrrolines, diamine, and amino alcohol was conducted. A sequential procedure involving acidic deprotection and reductive amination allows a rapid route to transform chiral sulfinamide into pyrroline. Fortunately, the good retention of the chiral center is observed; corresponding products **5** and **6** were afforded with 94% and 96% ee values, respectively. Noteworthy, chiral pyrroline **6** is a key intermediate for the anti-cancer medicine Larotrectinib[60] with an identical configuration. Furthermore, the direct reduction of corresponding products with excessive sodium borohydride gives direct access to chiral diamine (**7**) and amino alcohol (**8**).

Mechanism investigation

We conducted a series of cyclic voltammetry (CV) experiments to better understand the role of the [Co/K] bimetallic catalyst. Initially, the comparison of substrates' reductive potential illustrates that the electrophilic reactant **2a** and benzaldehyde are more susceptible to cathodic reduction than *N*-allylimine **1a** (Fig. 5a). This result verifies

Fig. 3 | Scope of terminal C–H functionalization of *N*-allylimine. Reaction conditions: **1** (1.5 mmol), **2** (0.5 mmol), **cat 2** (5 mol%), *^{n}*Bu$_4$NClO$_4$ (1.0 mmol), DMF (10 mL), graphite felt anode, nickel plate cathode, undivided cell, CCE = 18 mA, 3 h (4.03 F/mol), 0 °C; Yields were based on isolated products; dr > 15/1, unless otherwise noted. *^{a}*The reaction is conducted on a 0.3 mmol scale. GF graphite felt, CCE constant current electrolysis, DMF *N,N*-dimethylformamide.

that the Pinacol-type coupling between these substrates should be more favored without the intervention of a catalyst. Titrating substrates with **cat 2** resulted in contrasting results. For instance, treating **1a** with an increasing gradient of **cat 2** gives a surge of reductive peak

of **1a** (Fig. 5b). Conversely, no significant change was detected in the case of **2a** (Fig. S25). Mixing benzaldehyde with **cat 2** failed to boost the peak current, nor did it (Fig. S26). From these observations, we drew a conclusion that **cat 2** could selectively promote the HER of **1a** in the
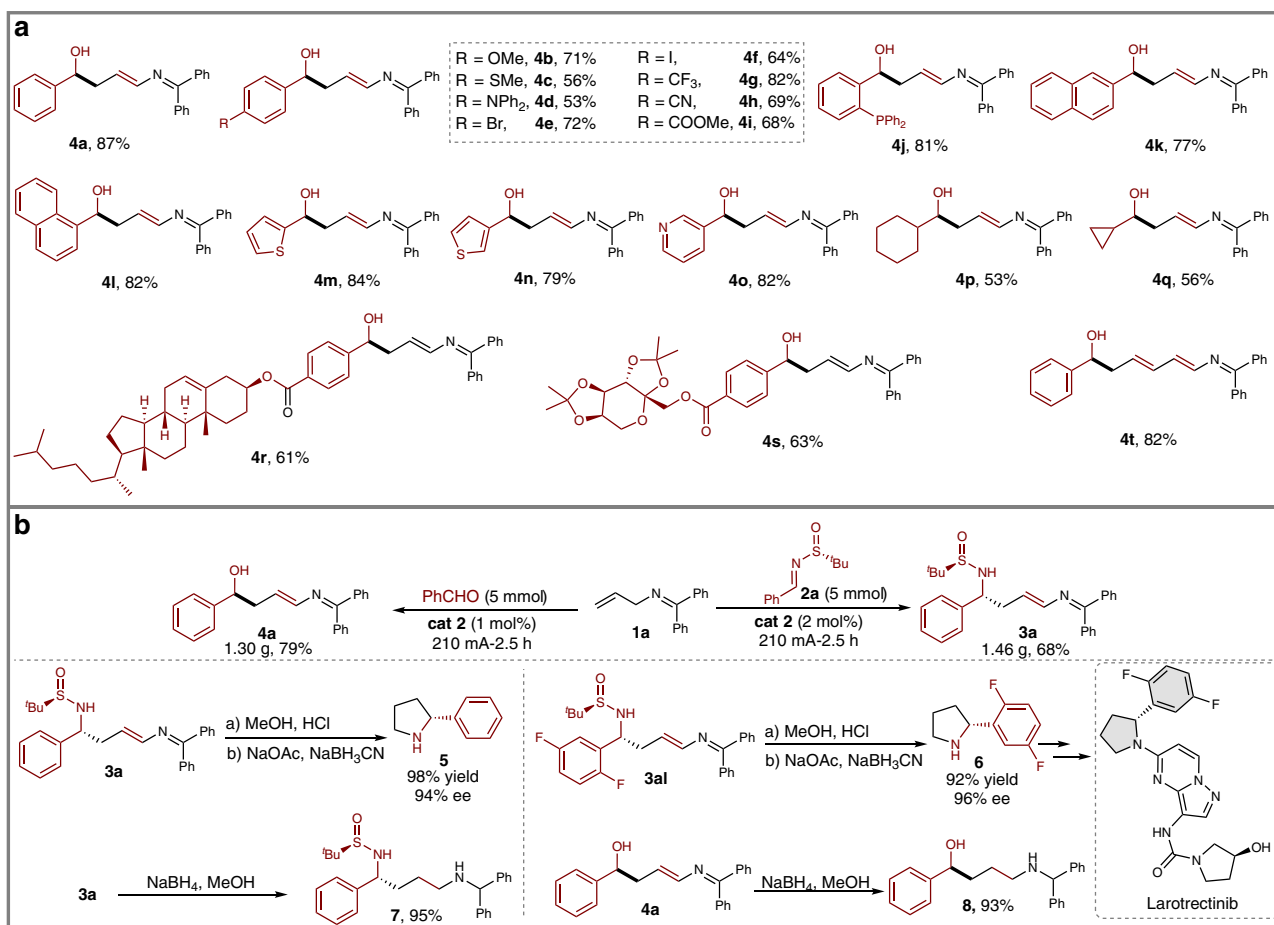
Fig. 4 | Utility of the [Co/K] catalyzed protocol. a Electrochemical terminal C–H functionalization of *N*-allylimine with aldehydes. **b** Gram-scale reaction and product derivatization.

presence of more reducible substrates **2a** and benzaldehyde. The naked base site of **cat 2** might be responsible for the selective interaction with the acidic allylic C–H bond of **1a**, thus facilitating the inner-sphere electron transfer for the HER of **1a**. Neither varying **1a** to the weakly acidic substrate **1bd** nor replacing **cat 2** with **cat 5** resulted in a significant increase in the cathodic peak current of the substrates (Figs. S27–S28), which evidenced the necessity of acid-base interaction. Further CV titration experiment of **cat 2** with excessive **1a** gave rise of a new noticeable peak at −1.58 V (Fig. 5c), which was tentatively ascribed to the in situ formed species **A** via deprotonation from **1a**. We validated this postulation by using acetic acid to replace **1a**, and an analogous peak emerged at the same position (Fig. 5d). Finally, the GC detection of hydrogen byproduct from the reaction supports the hydrogen evolution process of **1a** (Fig. S33). Taken together, bimetallic catalyst **cat 2** selectively enhanced the HER of **1a** by forming the reactive species **A**.

To further elucidate the reaction mechanism, various control experiments were carried out (Fig. 5e). We first ruled out the possible radical pathway by radical suppression (Eq. a) and radical clock experiments (Eq. b). Introducing excessive radical scavengers, such as 1,1-diphenylethene, 2,2,6,6-tetramethylperidinooxy (TEMPO), and triethyl phosphite, led to negligible changes in the reaction yield. Probing the reaction with the substrate **1be** only afforded the desired product **3be** without detecting any radical-initiated ring expansion product. This excludes the reaction mechanism triggered by the single-electron reduction of the imine moiety. We next confirmed the ionic pathway by a deuterium incorporation experiment (Eq. c). Treating the model reaction with 6 equivalents of deuterium oxide

(D$_2$O) gave a partially deuterated product **3a** in a diminished yield (9%). This result can be interpreted as the deuterium exchange of allyl carbanions during the reaction. Furthermore, the kinetic isotope effect (KIE) was studied to get insight into the rate-determining step (RDS). Mono-deuterated substrate **1a-D** was employed in the intramolecular competing experiment (Eq. d). Remarkably, the deuterium atom has been largely retained, and the ratio of k_H/k_D was determined to be 15.5/1, suggesting the C–H cleavage should be the RDS. Finally, we tried to simulate the in situ formed metal hydride species in the HER catalysis with sodium hydride as a surrogate (Eq. e). To our delight, the multistep procedure involving deprotonation and nucleophilic addition gave a single product **3a**, albeit with inferior yield (19%). This comparable selectivity confirms that the metal hydride should be the reactive species in the electrochemical reaction.

On the basis of the experimental observations and related mechanism[13] on bimetallic HER, a plausible reaction mechanism is proposed (Fig. 6a). The HER catalytic cycle is initiated by the Co^{II} species (**cat 2'**) via the cathodic reduction of its precatalyst **cat 2**. The naked carboxylate site promotes the proton dissociation from substrate **1a** to deliver a protonated species **A**, which leads to a further cathodic reduction and gives Co^{I} species **B**. With the high nucleophilicity of the Co^{I} center, intramolecular proton transfer occurs rapidly to yield a Co^{III} hydride **C**, in which the hydride bridges cobalt and alkali ions owing to its affinity to alkali metals. Subsequently, the single-electron reduction of **C** delivers more alkaline Co^{II} hydride **D**, and it facilitates further deprotonation of **1a**, releasing hydrogen and resonant carbanions **Int-I** and **Int-II**. Finally, the nucleophilic addition between the resulting carbanions and chiral imine **2a** affords the result
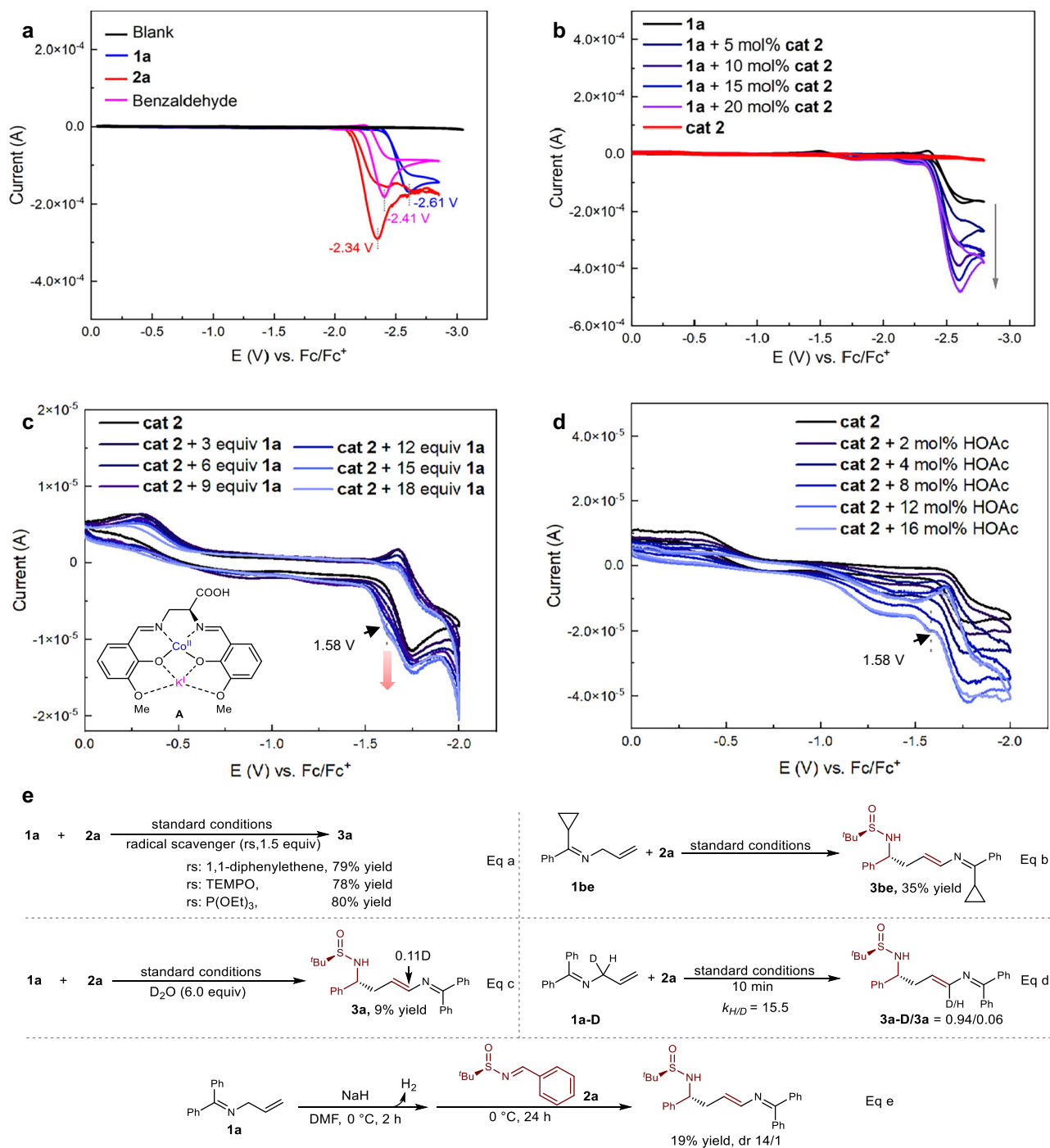
Fig. 5 | Cyclic voltammetry and control experiments. a Cyclic voltammogram of **1a** (0.05 mmol), **2a** (0.05 mmol) and benzaldehyde (0.05 mmol) in DMF (3.0 mL) solution with ^{n}BuNClO$_4$ as electrolyte. **b** Cyclic voltammogram of **1a** (0.05 mmol) and **cat 2** in DMF (3.0 mL) solution with ^{n}BuNClO$_4$ as electrolyte. **c** Cyclic voltammogram of **cat 2** (0.01 mmol) and **1a** in DMF (3.0 mL) solution with ^{n}BuNClO$_4$ as electrolyte. **d** Cyclic voltammogram of **cat 2** (0.01 mmol) and HOAc in DMF (3.0 mL) solution with ^{n}BuNClO$_4$ as electrolyte. **e** Control experiments. Fc ferrocene, DMF *N,N*-dimethylformamide, TEMPO 2,2,6,6-Tetramethylpiperidinooxy.

product **3a** and a possible branched product **3a-1**. Noteworthy, the dimeric form of the catalytic species (**cat 2′**, **C** and **D**) may participate in the catalytic cycle due to strong interactions between the carboxylate moiety and the K⁺ ion of a neighboring molecule. On the anode side, the oxidation of the DMF should be the predominant reaction based on the cyclic voltammetry experiment (Fig. S31).

We rationalized the effect of alkali metals on the HER performance by density functional theory (DFT) calculations (Fig. 6b). The results illustrate that alkalic metals significantly affect the structure of the Co^{II}

catalysts (**cat′**) and their transformation into the intermediate **D**. Specifically, Na and K ions result in nearly planar geometry in catalysts **cat 1′**-**cat 2′** with dihedral (K-O-Co-O) ranging from 1.7 to 3.3°. In contrast, the larger Rb and Cs ions lead to bowed structures (dihedrals 15.9–26.3°), which would introduces pronounced steric hindrance for the formation of the hydride species **D**. Transition-state calculations (Figs. S45–S48) validate that larger alkali metals correspond to higher energy barriers (1.90–5.83 kcal/mol), indicating a more sluggish process for the generation of intermediate **D** based on the further rate constant
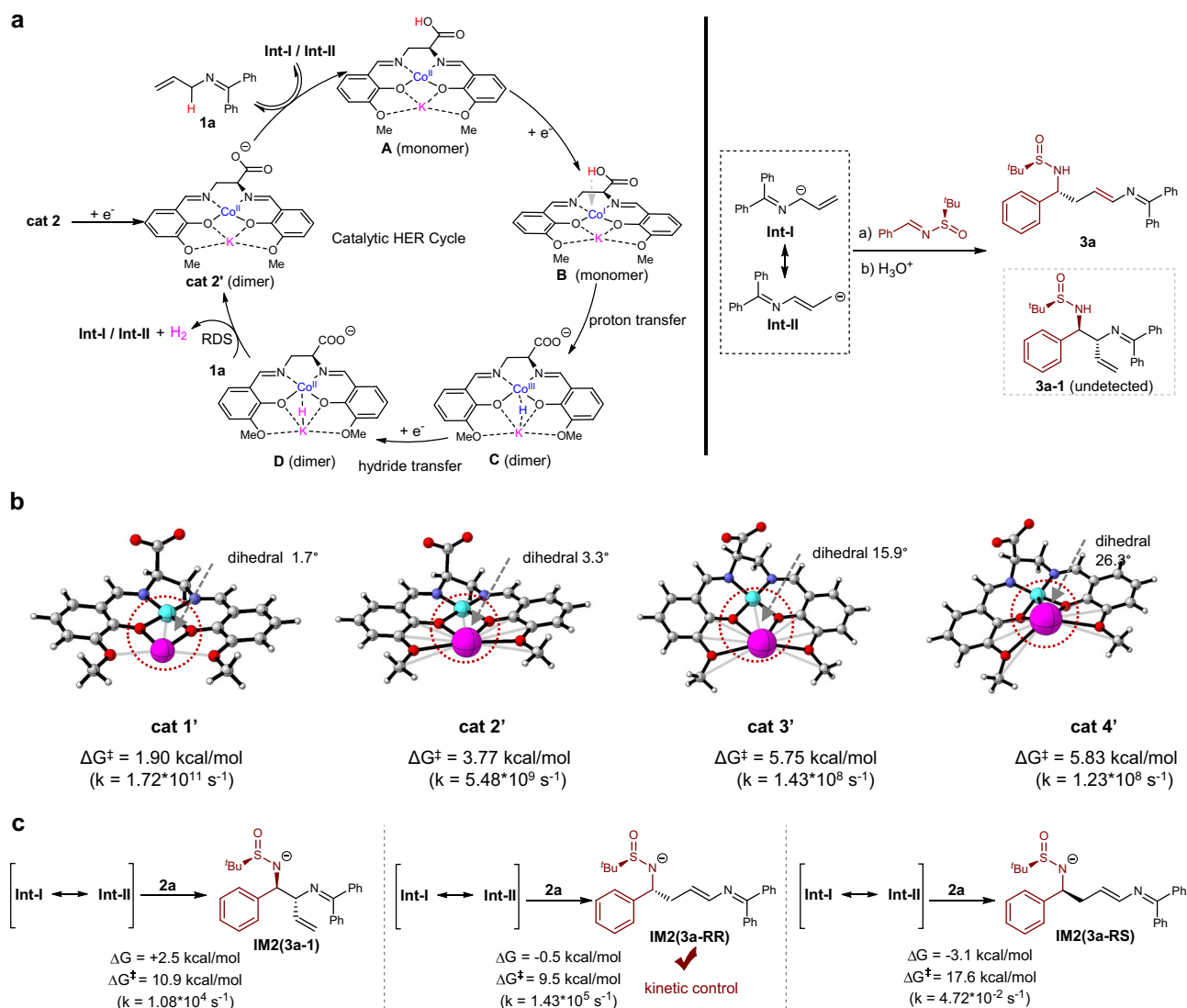
Fig. 6 | Reaction mechanism. a Proposed catalytic cycle for the electrochemical functionalization. **b** DFT calculations for the catalytic species. **c** DFT calculations for the nucleophilic addition between carbanions and Ellman imine. DFT density functional theory.

calculation[61]. The alkalinity of the in situ formed metal hydrides is the other factor for the HER efficiency, which has a positive correlation with the alkali metallicity. Consequently, the superior catalytic performance of the potassium-based catalyst (**cat 2**) can be attributed to its optimal ionic radius and the reasonable alkalinity of its metal hydride intermediate. Moreover, the DFT calculations (Fig. S49) for the reaction between carbanions **Int-I/Int-II** and imine **2a** rationalize that the carbanion adduct **IM2(3a-RR)** is a kinetic control product with the lowest reaction activation energy of 9.5 kcal/mol (Fig. 6c).

Discussion

In summary, we have developed an array of bimetallic HER catalysts by incorporating redox-active cobalt centers with alkali metal ions. These combinations significantly enhance HER performance, enabling the terminal C−H selectivity in the functionalization of N-allylimines. With a naked base site in the bimetallic catalyst, the HER of N-allylimines is promoted to outcompete the undesired reductive coupling, thereby providing broad access to chiral amine products. DFT calculations and control experiments reveal that the enhancement of HER performance by alkali metals is dictated by their ion radius and metallicity. Our laboratory is actively exploring the repurposing of these bimetallic HER catalysts to solve the challenges in synthetic chemistry.

Methods

General procedure for electrochemical terminal C−H functionalization of N-Allylimine

An undivided cell was equipped with a magnetic stirrer, nickel plate (1.8*1.5 cm^2), graphite felt (1.8*1.5 cm^2), as cathode and anode, respectively (the electrolysis setup is shown in Fig. S35). The substrate N-allylimine **1a** (332 mg, 1.5 mmol), Ellman imine **2a** (105 mg, 0.5 mmol), **cat 2** (12 mg, 0.025 mmol), and ^{n}Bu$_4$NClO$_4$ (342 mg, 1.0 mmol) were added to the solvent DMF (10 mL). The resulting mixture was allowed to stir and electrolyze under constant current conditions (18 mA, $J = 6.7$ mA•cm^{-2}) at 0 °C for 3 h. The reaction mixture was subsequently poured into water (200 mL) and extracted with ethyl acetate (40 mL*3). The combined organic phases were washed with saturated brine solution (100 mL). The volatile solvent was then removed with a rotary evaporator, and the residue was purified by column chromatography (PE/EA = 5/1−2/1, v/v basified with 1% triethylamine) on silica gel to afford the desired product **3a** (174 mg) in 81% yield.

Data availability

All data supporting the findings of this study, including experimental details, spectroscopic characterization data for all compounds, are available in the text and the Supplementary Information section.

Crystallographic data for the structure reported in this article have been deposited at the Cambridge Crystallographic Data Centre, under deposition numbers CCDC 2422475 (**cat 2**). Copies of the data can be obtained free of charge via https://www.ccdc.cam.ac.uk/structures/. All data are available from the corresponding author upon request. All of the original figure data in this study are provided in the Source Data file. The Cartesian coordinates generated in the DFT calculation are provided in Supplementary Data 1. Source data are provided with this paper.

References

1. Koper, M. T. M. & Bouwman, E. Electrochemical hydrogen production: bridging homogeneous and heterogeneous catalysis. *Angew. Chem. Int. Ed.* **49**, 3723–3725 (2010).
2. McKone, J. R., Marinescu, S. C., Brunchwig, B. S., Winkler, J. R. & Gray, H. B. Earth-abundant hydrogen evolution electrocatalysts. *Chem. Sci.* **5**, 865–878 (2014).
3. Zhu, J., Hu, L., Zhao, P., Lee, L. Y. S. & Wong, K.-Y. Recent advances in electrocatalytic hydrogen evolution using nanoparticles. *Chem. Rev.* **120**, 851–918 (2020).
4. Zheng, Y., Jiao, Y., Vasileff, A. & Qiao, S.-Z. The hydrogen evolution reaction in alkaline solution: from theory, single crystal models, to practical electrocatalysts. *Angew. Chem. Int. Ed.* **57**, 7568–7579 (2018).
5. Tard, C. & Pickett, C. J. Structural and functional analogues of the active sites of the [Fe]-, [NiFe]-, and [FeFe]-hydrogenases. *Chem. Rev.* **109**, 2245–2274 (2009).
6. Tai, H., Hirota, S. & Stripp, S. T. Proton transfer mechanisms in bimetallic hydrogenases. *Acc. Chem. Res.* **54**, 232–241 (2021).
7. Wang, F. et al. Selective functionalization of alkenes and alkynes by dinuclear manganese catalysts. *Acc. Chem. Res.* **57**, 2985–3006 (2024).
8. Chen, K. et al. Switch in selectivities by dinuclear nickel catalysis: 1,4-hydroarylation of 1,3-dienes to Z-olefins. *J. Am. Chem. Soc.* **145**, 24877–24888 (2023).
9. Chen, Q.-F., Xiao, Y., Hua, K., Zhang, H.-T. & Zhang, M.-T. Bimetallic synergy in oxygen reduction: how tailored metal–metal interactions amplify cooperative catalysis. *J. Am. Chem. Soc.* **147**, 14504–14518 (2025).
10. Peng, P. et al. Unlocking the nucleophilicity of strong alkyl C–H bonds via Cu/Cr catalysis. *ACS Cent. Sci.* **9**, 756–762 (2023).
11. Wei, Z., Sun, J., Li, Y., Datyte, A. K. & Wang, Y. Bimetallic catalysts for hydrogen generation. *Chem. Soc. Rev.* **41**, 7994–8008 (2012).
12. Liu, L. & Corma, A. Bimetallic sites for catalysis: from binuclear metal sites to bimetallic nanoclusters and nanoparticles. *Chem. Rev.* **123**, 4855–4933 (2023).
13. Brazzolotto, D. et al. Nickel-centred proton reduction catalysis in a model of [NiFe] hydrogenase. *Nat. Chem.* **8**, 1054–1060 (2016).
14. Cloward, I. N. et al. Catalyst self-assembly accelerates bimetallic light-driven electrocatalytic H$_2$ evolution in water. *Nat. Chem.* **16**, 709–716 (2024).
15. Valdez, C. N., Dempsey, J. L., Brunschwig, B. S., Winkler, J. R. & Gray, H. B. Catalytic hydrogen evolution from a covalently linked dicobaloxime. *Proc. Natl. Acad. Sci. USA* **109**, 15589–15593 (2012).
16. Bullock, R. M. & Helm, M. L. Molecular electrocatalysts for oxidation of hydrogen using earth-abundant metals: shoving protons around with proton relays. *Acc. Chem. Res.* **48**, 2017–2026 (2015).
17. Haake, M., Reuillard, B., Chavarot-Kerlidou, M., Costentin, C. & Artero, V. Proton relays in molecular catalysis for hydrogen evolution and oxidation: lessons from the mimicry of hydrogenases and electrochemical kinetic analyses. *Angew. Chem. Int. Ed.* **63**, e202413910 (2024).
18. Barton, B. E., Olsen, M. T. & Rauchfuss, T. B. Aza- and oxadithiolates are probable proton relays in functional models for the [FeFe]-hydrogenases. *J. Am. Chem. Soc.* **130**, 16834–16835 (2008).
19. Helm, M. L., Stewart, M. P., Bullock, R. M., DuBois, M. R. & DuBois, D. L. A synthetic nickel electrocatalyst with a turnover frequency above 100,000 s^{-1} for H$_2$ production. *Science* **333**, 863–866 (2011).
20. Bediako, D. K. et al. Role of pendant proton relays and proton-coupled electron transfer on the hydrogen evolution reaction by nickel hangman porphyrins. *Proc. Natl. Acad. Sci. USA* **111**, 15001–15006 (2014).
21. Queyriaux, N. et al. Electrocatalytic hydrogen evolution with a cobalt complex bearing pendant proton relays: acid strength and applied potential govern mechanism and stability. *J. Am. Chem. Soc.* **142**, 274–282 (2020).
22. Lin, S. et al. Electrochemical strategy for proton relay installation enhances the activity of a hydrogen evolution electrocatalyst. *J. Am. Chem. Soc.* **144**, 20267–20277 (2022).
23. Zhang, S. et al. Electrochemically generated carbanions enable isomerizing allylation and allenylation of aldehydes with alkenes and alkynes. *J. Am. Chem. Soc.* **145**, 14143–14154 (2023).
24. Liang, Y. et al. A hydrogen evolution catalyst [Co$_2$O$_2$] metallacycle enables regioselective allene C(sp^2)-H functionalization. *Angew. Chem. Int. Ed.* **63**, e202400938 (2024).
25. Liu, K. et al. Paired electrocatalysis unlocks cross-dehydrogenative coupling of C(sp^3)-H bonds using a pentacoordinated cobalt-salen catalyst. *Nat. Commun.* **15**, 2897 (2024).
26. Feng, J. et al. Electrochemical allene C—H functionalization via carbanion sampling. *Angew. Chem. Int. Ed.* **64**, e202508369 (2025).
27. Song, L. et al. Dual electrocatalysis enables enantioselective hydrocyanation of conjugated alkenes. *Nat. Chem.* **12**, 747–754 (2020).
28. Cai, C.-Y. et al. Tailored cobalt-salen complexes enable electrocatalytic intramolecular allylic C–H functionalizations. *Nat. Commun.* **12**, 3745 (2021).
29. Chen, M., Wu, Z.-J., Song, J. & Xu, H.-C. Electrocatalytic allylic C–H alkylation enabled by a dual-function cobalt catalyst. *Angew. Chem. Int. Ed.* **61**, e202115954 (2022).
30. Yang, F. et al. Electrocatalytic oxidative hydrofunctionalization reactions of alkenes via Co(II/III/IV) cycle. *ACS Catal.* **12**, 2132–2137 (2022).
31. Huang, C., Tao, Y., Cao, X., Zhou, C. & Lu, Q. Asymmetric paired electrocatalysis: enantioselective olefin–sulfonylimine coupling. *J. Am. Chem. Soc.* **146**, 1984–1991 (2024).
32. Shah, A. H. et al. The role of alkali metal cations and platinum-surface hydroxyl in the alkaline hydrogen evolution reaction. *Nat. Catal.* **5**, 923–933 (2022).
33. Ji, S. G. et al. Alkali metal cations act as homogeneous cocatalysts for the oxygen reduction reaction in aqueous electrolytes. *Nat. Catal.* **7**, 1330–1338 (2024).
34. Zhang, S. & Li, M.-B. Repurposing HER catalysis toward metal hydride-mediated electro-reductive transformations. *Tetrahedron Chem.* **11**, 100080 (2024).
35. Gnaim, S. et al. Cobalt-electrocatalytic HAT for functionalization of unsaturated C–C bonds. *Nature* **605**, 687–695 (2022).
36. Wu, X. et al. Intercepting hydrogen evolution with hydrogen-atom transfer: electron-initiated hydrofunctionalization of alkenes. *J. Am. Chem. Soc.* **144**, 17783–17791 (2022).
37. Derosa, J., Garrido-Barros, P., Li, M. & Peters, J. C. Use of a PCET mediator enables a Ni-HER electrocatalyst to act as a hydride delivery agent. *J. Am. Chem. Soc.* **144**, 20118–20125 (2022).
38. Liu, C., Wu, Y., Zhao, B. & Zhang, B. Designed nanomaterials for electrocatalytic organic hydrogenation using water as the hydrogen source. *Acc. Chem. Res.* **56**, 1872–1883 (2023).
39. Wang, T., He, F., Jiang, W. & Liu, J. Electrohydrogenation of nitriles with amines by cobalt catalysis. *Angew. Chem. Int. Ed.* **63**, e202316140 (2024).

40. Wang, Y. et al. Electroreduction of unactivated alkenes using water as hydrogen source. *Nat. Commun.* **15**, 2780 (2024).
41. Yan, M., Kawamata, Y. & Baran, P. S. Synthetic organic electrochemical methods since 2000: on the verge of a renaissance. *Chem. Rev.* **117**, 13230–13319 (2017).
42. Yuan, Y. & Lei, A. Electrochemical oxidative cross-coupling with hydrogen evolution reactions. *Acc. Chem. Res.* **52**, 3309–3324 (2019).
43. Jiao, K.-J., Xing, Y.-K., Yang, Q.-L., Qiu, H. & Mei, T.-S. Site-selective C–H functionalization via synergistic use of electrochemistry and transition metal catalysis. *Acc. Chem. Res.* **53**, 300–310 (2020).
44. Li, P., Wang, Y., Zhao, H. & Qiu, Y. Electroreductive cross-coupling reactions: carboxylation, deuteration, and alkylation. *Acc. Chem. Res.* **58**, 113–129 (2025).
45. Xiong, P. & Xu, H.-C. Molecular photoelectrocatalysis for radical reactions. *Acc. Chem. Res.* **58**, 299–311 (2025).
46. Zhang, Q., Liang, K. & Guo, C. Enantioselective nickel-catalyzed electrochemical radical allylation. *Angew. Chem. Int. Ed.* **61**, e202210632 (2022).
47. Shi, A., Xie, P., Wang, Y. & Qiu, Y. Photoelectrocatalytic Cl-mediated $C(sp^3)$–H aminomethylation of hydrocarbons by $BiVO_4$ photoanodes. *Nat. Commun.* **16**, 2322 (2025).
48. Wang, T.-C. et al. Palladium-catalyzed enantioselective $C(sp^3)$–H/$C(sp^3)$–H umpolung coupling of N-allylimine and α-Aryl ketones. *J. Am. Chem. Soc.* **143**, 20454–20461 (2021).
49. Fan, X., Gong, X., Ma, M., Wang, R. & Walsh, P. J. Visible light-promoted CO_2 fixation with imines to synthesize diaryl α-amino acids. *Nat. Commun.* **9**, 4936 (2018).
50. Pan, Z.-Z., Li, J.-H., Tian, H. & Yin, L. Copper(I)-catalyzed asymmetric allylation of ketones with 2-aza-1,4-dienes. *Angew. Chem. Int. Ed.* **63**, e202315293 (2024).
51. Daniel, P. E., Weber, A. E. & Malcolmson, S. J. Umpolung synthesis of 1,3-amino alcohols: stereoselective addition of 2-azaallyl anions to epoxides. *Org. Lett.* **19**, 3490–3493 (2017).
52. Uphade, M. B., Reddy, A. A., Khandare, S. P. & Prasad, K. R. Stereoselective addition of a lithium anion of 1,1-diphenyl-2-aza-pentadiene to sulfinimines: application to the synthesis of (–)-epiquinamide. *Org. Lett.* **21**, 9109–9113 (2019).
53. Marshall, C. M., Federice, J. G., Bell, C. N., Cox, P. B. & Njardarson, J. T. An update on the nitrogen heterocycle compositions and properties of U.S. FDA-approved pharmaceuticals (2013–2023). *J. Med. Chem.* **67**, 11622–11655 (2024).
54. Jensen, K. L., Dickmeiss, G., Jiang, H., Albrecht, Ł & Jørgensen, K. A. The diarylprolinol silyl ether system: a general organocatalyst. *Acc. Chem. Res.* **45**, 248–264 (2012).
55. Zhang, S. et al. Catalyst-dependent direct and deoxygenative coupling of alcohols by convergent paired electrolysis. *CCS Chem.* **4**, 1938–1948 (2022).
56. Wang, L.-J., Ye, P., Tan, N. & Zhang, B. Electroreductive cross-coupling between aldehydes and ketones or imines via cathodically generated dianions. *Green. Chem.* **24**, 8386–8392 (2022).
57. Kwak, D. et al. Electroreductive access to 1,2-aminoalcohols via cross aza-pinacol coupling of N-acyl diarylketimines and aldehydes. *Org. Lett.* **26**, 2733–2738 (2024).
58. Deacy, A. C., Moreby, E., Phanopoulos, A. & Willams, C. K. Co(III)/alkali-metal(i) heterodinuclear catalysts for the ring-opening copolymerization of CO_2 and propylene oxide. *J. Am. Chem. Soc.* **142**, 19150–19160 (2020).
59. Ellman, J. A., Owens, T. D. & Tang, T. P. *N-tert*-butanesulfinyl imines: versatile intermediates for the asymmetric synthesis of amines. *Acc. Chem. Res.* **35**, 984–995 (2002).
60. Bernhard, L. M., McLachlan, J. & Gröger, H. Process development of enantioselective imine reductase-catalyzed syntheses of pharmaceutically relevant pyrrolidines. *Org. Process Res. Dev.* **26**, 2067–2074 (2022).
61. Eyring, H. The activated complex in chemical reactions. *J. Chem. Phys.* **3**, 107–115 (1935).

Acknowledgements

Author contributions
S.Z. and M.-B.L. conceived the project, designed the experiments, and wrote the manuscript. S.Z., L.H., and M.W. performed the experimental work. J.F. and J.H. carried out a density functional theory calculation. Refinement and analysis of single-crystal data was conducted by Y.Z. All authors discussed the results and commented on the manuscript.

Competing interests
The authors declare no competing interests.

Additional information
Supplementary information The online version contains supplementary material available at https://doi.org/10.1038/s41467-025-63914-0.

Correspondence and requests for materials should be addressed to Sheng Zhang or Man-Bo Li.

Peer review information *Nature Communications* thanks Silvia Bordoni, who co-reviewed with Federico MoroPraveena Gopalan and Hai-Chao Xu for their contribution to the peer review of this work. A peer review file is available.

Reprints and permissions information is available at http://www.nature.com/reprints

Publisher's note Springer Nature remains neutral with regard to jurisdictional claims in published maps and institutional affiliations.